Self-organization in Turbulent Molecular Clouds: Compressional versus Solenoidal Modes

A. G. Kritsuk[1], S. D. Ustyugov[2], M. L. Norman[1], and P. Padoan[1]

Abstract. We use three-dimensional numerical simulations to study self-organization in supersonic turbulence in molecular clouds. Our numerical experiments describe decaying and driven turbulent flows with an isothermal equation of state, sonic Mach numbers from 2 to 10, and various degrees of magnetization. We focus on properties of the velocity field and, specifically, on the level of its potential (dilatational) component as a function of turbulent Mach number, magnetic field strength, and scale. We show how extreme choices of either purely solenoidal or purely potential forcing can reduce the extent of the inertial range in the context of periodic box models for molecular cloud turbulence. We suggest an optimized forcing to maximize the effective Reynolds number in numerical models.

1. Introduction

Modern statistical theories of fragmentation of molecular clouds (MCs) and star formation are based on an interpretation of the non-thermal emission linewidths and their correlation with length scale in terms of supersonic turbulence (Kaplan & Pronik 1953; Larson 1981; Heyer & Brunt 2004). It is believed that both the star formation rate and the initial mass function of newly born stars are controlled by MC turbulence (e.g., Padoan et al. 2007; McKee & Ostriker 2007; Padoan & Nordlund 2009). There are competing views on the origin of this turbulence, which is either explained as a transient phenomenon associated with the cloud formation process or as if it were continuously driven by various energy sources (e.g., differential rotation, supernovae, stellar winds, protostellar outflows, variable FUV background, etc. (Mac Low & Klessen 2004)). Since the typical Reynolds numbers in MCs are $\sim 10^8$, expectations to find purely laminar regions in the cold star forming molecular gas on scales from ~ 50 pc down to a few astronomical units should be pretty low (Elmegreen & Scalo 2004).

The supersonic regime typical of MC turbulence is extremely hard to achieve in the laboratory and the information available from astronomical observations is limited (e.g., Heyer & Brunt 2004). Most of what we know about the statistics of supersonic turbulence comes from large-scale numerical experiments intended to reproduce the basic non-linear processes operating in the energy cascade in the inertial range of scales (e.g., Kritsuk et al. 2007a). The effective Reynolds

[1]Physics Department and Center for Astrophysics & Space Sciences, University of California, San Diego; 9500 Gilman Drive, La Jolla, CA 92093-0424, USA

[2]Keldysh Institute for Applied Mathematics, Russian Academy of Sciences, Miusskaya Pl. 4, Moscow 125047, Russia

numbers normally achieved in such simulations are at most $\sim 10^4$, i.e. much smaller than the realistic values. Since computational resources are always limited, even with the most advanced and least dissipative numerical methods only a short stretch of the inertial interval can be captured at current grid resolutions up to 2048^3 zones (Kritsuk et al. 2009a). Simulations also rely on a number of assumptions intended to simplify the model and make it more tractable, such as the periodic boundary conditions and an isothermal equation of state. To achieve a better scale separation, an approach of implicit large eddy simulations (ILES) is used (Sytine et al. 2000). The effects of molecular viscosity are, thus, replaced by numerical diffusivity of purely artificial nature. In simulations involving magnetic fields, the magnetic diffusivity is also replaced by the effective one built into an ideal MHD solver in use. In these circumstances the effective magnetic Prandtl numbers usually achieved are on the order unity (e.g., Kritsuk et al. 2009b).

The assumption of isothermality naturally restricts the physical box size to $L \lesssim 5$ pc, as the presence of multiple thermal phases plays a role on larger scales. In these circumstances, an artificial stirring force is required to mimic the turbulent energy flux from larger-scale cascade that cannot be modeled directly due to a finite physical dimension of the computational domain. With some rare exceptions, most of the models rely on a purely solenoidal forcing on large scales to provide a better 'boundary condition' for the inertial interval in the wavenumber space (e.g., Boldyrev et al. 2002a). While the stellar energy sources would mostly generate compressive fluctuations, the choice of a solenoidal force was then justified by the small compressional-to-solenoidal ratio measured in simulations.

With higher quality and larger simulations available today, we can now reassess the domain of applicability of solenoidal forcing in isothermal simulations of MC turbulence. To achieve this goal, we use various simulations we have performed in the past to investigate self-organization in supersonic turbulence and quantify the equilibrium compressional-to-solenoidal ratio in the inertial range as a function of the sonic and Alfvénic Mach numbers. We then come up with an optimized prescription for the large-scale forcing in isothermal periodic boxes that allows us to achieve a better scale separation. We show that a poor choice of forcing parameterization can easily lead to a complete elimination of the inertial range and result in rather "pathological" statistics, which have nothing to do with turbulence that fully develops far from boundaries and external forces at very high Reynolds numbers.

2.   Dilatational and solenoidal motions in supersonic turbulence

The velocity field $\mathbf{u}(x,t)$ can be decomposed into solenoidal and dilatational parts $\mathbf{u}_s$ and $\mathbf{u}_c$, such that $\mathbf{u} = \mathbf{u}_s + \mathbf{u}_c$, $\nabla \cdot \mathbf{u}_s = 0$ and $\nabla \times \mathbf{u}_c = 0$ via Helmholtz decomposition. Let us consider $\chi(k) \equiv P(\mathbf{u}_c, k)/P(\mathbf{u}_s, k)$ as a measure of the flow compressibility,[1] where $P(\mathbf{a}, k)$ is the three-dimensional power spectrum of a vector field $\mathbf{a}$, and k is the wavenumber. In an incompressible fluid $\chi(k) \equiv 0$,

---

[1]There are also alternative measures of compressibility, e.g. $\gamma \equiv \langle u_c^2 \rangle / \langle u_s^2 \rangle$, which gives the global ratio of the specific kinetic energy contained in the dilatational and solenoidal modes;

while in a compressible gaseous medium with purely potential (rotation-free) velocity field $\chi(k) \equiv \infty$.

In fully developed supersonic isothermal turbulence, $\chi(k)$ describes a balance established via nonlinear exchange between the dilatational and solenoidal modes, which is ultimately controlled by the sonic (M_s) and Alfvénic (M_A) Mach numbers. In non-magnetized flows ($M_A = \infty$) at low sonic Mach numbers ($M_s \ll 1$), compressibility is very weak and $\chi(k)$ tends to settle at zero. At high turbulent Mach numbers ($M_s \gg 1$), the compressional-to-solenoidal ratio hovers around $1 : 2$, which can be explained by simple geometrical considerations (e.g., Nordlund & Padoan 2003). In MHD turbulence, the natural tendency towards Alfvénization, or dynamic alignment between the velocity field **u** and the divergence-free magnetic field **B** in the bulk of the volume away from shocks and dynamic rarefactions, results in suppression of dilatational activity. Thus, the presence of dynamically important magnetic fields would effectively reduce $\chi(k)$ in trans- and sub-Alfvénic turbulence (e.g., Boldyrev et al. 2002a).

In simulations, besides M_s and M_A, the ratio $\chi(k)$ would also depend on the content of solenoidal and dilatational modes in the large-scale forcing, χ_f. If χ_f is far from the equilibrium ratio that corresponds to chosen values of M_s and M_A, the effect of such forcing will be felt further down the hierarchy of scales and the inertial range in such simulations would shrink or disappear depending on what χ_f is enforced at the driving scale k_f. Most of the simulations conservatively used a purely solenoidal forcing with $\chi_f = 0$, with the exception of $\chi_f \approx 0.7$ in Kritsuk et al. (2007a). Schmidt et al. (2008) recently considered both $\chi_f = 0$ and $\chi_f = \infty$ in 1024^3 non-magnetized simulations at $M_s \approx 5.5$ and found that the velocity scaling varies substantially with the large-scale forcing. Federrath et al. (2008) also discovered that the density pdf in their compressively driven models does not bear a lognormal shape, see also Schmidt et al. (2009). Federrath et al. (2009) showed that $\chi(k) \approx 1.2$ at $k/k_{min} \in [3, 70]$ in their 1024^3 simulation at $\chi_f = \infty$, while at $\chi_f = 0$ they obtained the expected $\chi(k) \approx 0.5$ at $k/k_{min} \in [8, 30]$, where $k_{min} = 2\pi$.[2] Schmidt (2009) found that a transition from $\chi_f = 0$ to $\chi_f = \infty$ causes strong variations in spectral properties of turbulence in his large eddy simulations (LES). While these "pathological" statistics observed in simulations with purely compressive forcing clearly indicate a complete absence of an inertial range even at a grid resolution of 1024^3 zones at $\chi_f = \infty$, they also hint at a possibility to optimize the problem setup by tuning the forcing to match the expected statistical equilibrium in the inertial range determined by the flow parameters. This would help to maximize the extent of the inertial range and thus to provide higher effective Reynolds numbers at the same computational cost.

$\chi_c(k) \equiv P(\mathbf{u}_c, k)/P(\mathbf{u}, k)$, which estimates the fraction of dilatational modes in the velocity power spectrum as a function of k; and $r_{cs} \equiv \langle |\nabla \cdot \mathbf{u}|^2 \rangle / (\langle |\nabla \cdot \mathbf{u}|^2 \rangle + \langle |\nabla \times \mathbf{u}|^2 \rangle)$, which represents the small-scale compressive ratio. Both χ_c and r_{cs} are bounded in the interval $[0, 1]$, while χ and γ can potentially take arbitrary positive values.

[2] The same simulations also produced an unusual peak in $\chi(k)$ on small scales at $k/k_{min} \in [300, 400]$ with the peak values of 2.3 and 4.0 in the runs with solenoidal and compressive forcing, respectively.
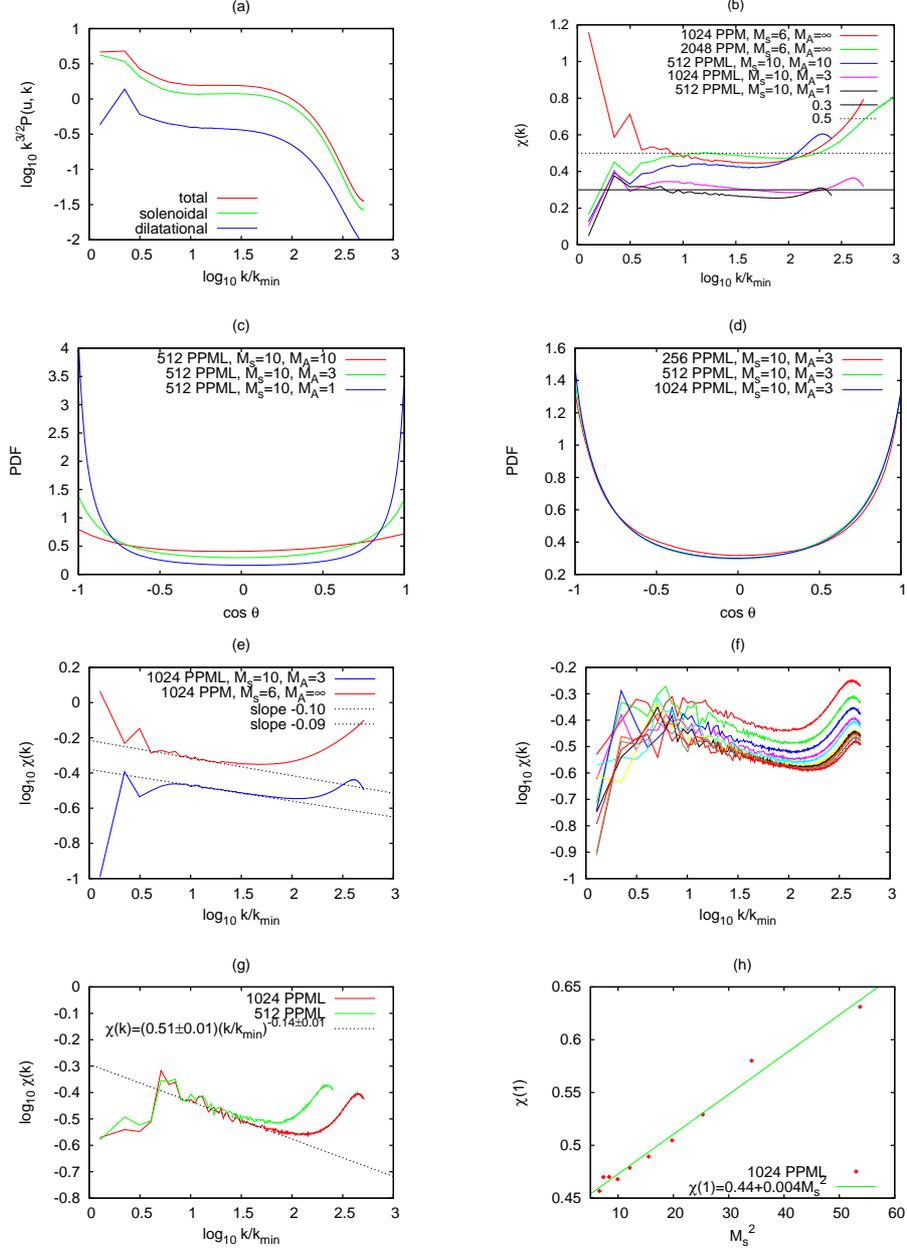
Figure 1.   Statistics of supersonic turbulence from simulations with PPM and PPML: (**a**) velocity power spectrum, and spectra for dilatational and solenoidal parts, $M_s = 10$ and $M_A = 3$; (**b**) $\chi(k)$ for simulations with mixed forcing ($\chi_f = 0.7$, red line) and with solenoidal forcing ($\chi_f = 0$, all the rest); (**c**) pdfs of the alignment angle for three 512^3 simulations with $M_A = 1$, 3, and 10; (**d**) convergence of the $\cos\theta$ pdfs for runs at 256^3, 512^3, and 1024^3; (**e**) same as (**b**), but for $log_{10}\chi(k)$ at 1024^3 only; (**f**) $\chi(k)$ for 10 snapshots from a 1024^3 simulation of turbulence decay; (**g**) convergence of $\chi(k)$ for the 5th snapshot from 512^3 and 1024^3 decay simulations; (**h**) $\chi(k/k_{min} = 1)$ as a function of M_s^2 from a 1024^3 simulation of turbulence decay.

To explore the effects of artificial large-scale forcing on the velocity field statistics at scales adjacent to the forcing range, we collected data from various isothermal simulations with and without magnetic fields (Kritsuk et al. 2007a, 2009a,b). The nonmagnetized runs utilized the Piecewise Parabolic Method (PPM) of Colella & Woodward (1984) implemented in the ENZO code.[3] The MHD simulations were carried out with our Piecewise Parabolic Method on a Local Stencil (PPML, Ustyugov et al. 2009).

Figure 1**a** gives an example of the velocity power spectrum $P(\mathbf{u}, k)$ and products of Helmholtz decomposition for a 1024^3 simulation with $\chi_f = 0$, $M_s = 10$ and $M_A = 3$ (Kritsuk et al. 2009b). One advantage of MHD simulations, even in the super-Alfvénic regime, where the weak field is dynamically unimportant in most of the simulation domain, is the absence of visible bottleneck contamination in the inertial subrange adjacent to the dissipation range. This simplifies the discussion of the inertial range scaling for $\chi(k)$. In Fig. 1**b** we collect the $\chi(k)$ functions from various simulations. For instance, the red and green curves represent two non-magnetized simulations with PPM at $M_s = 6$ with $\chi_f = 0.7$ (1024^3, Kritsuk et al. 2007a) and with $\chi_f = 0$ (2048^3, Kritsuk et al. 2009a). In both cases $\chi(k)$ is close to the asymptotic value of 0.5 at wavenumbers $k/k_{min} \in [10, 100]$, as expected. Similar χ-levels were also achieved in solenoidally driven non-magnetized simulations at $M_s \gtrsim 5$ by others (Pavlovski et al. 2006; Schmidt et al. 2009). Consistently lower levels of $\chi \lesssim 0.15$ were found in (adiabatic) simulations at $M_s \approx 1$ (Pouquet et al. 1991; Porter et al. 1994, 1999, 2002). As the strength of magnetic field fluctuations climbs up to equipartition with turbulent kinetic energy in our sequence of PPML simulations with $M_A = 10, 3$, and 1, the average level of χ drops from 0.5 to below 0.3 for the sonic Mach number fixed at $M_s = 10$ (see also Boldyrev et al. 2002a,b).

To illustrate the effects of dynamic alignment in magnetized supersonic flows, in Fig. 1**c** we show the probability density functions (pdfs) of the cosine of the alignment angle, $\cos\theta \equiv \mathbf{u} \cdot \mathbf{B}/\sqrt{u^2 B^2}$, for three 512^3 PPML simulations at $M_s = 10$ and $M_A = 10, 3$, and 1. In the most super-Alfvénic case at $M_A = 10$, the alignment is rather weak. It gets substantially stronger at $M_A = 1$, when the equipartition of turbulent magnetic and kinetic energies is reached. Fig, 1**d** shows that the pdf of the alignment angle is well converged already at resolution of 512^3 in a series of representative numerical experiments with $M_A = 3$ and grid resolutions of 256^3, 512^3, and 1024^3.

Let us get back to Fig. 1**b** and look at the shape of the compressional-to-solenoidal ratio $\chi(k)$ in more detail. Since the two non-magnetized (PPM) simulations differ only in χ_f and in the grid resolution, time-average spectra in Fig. 1**b** indeed capture the effects of large-scale forcing that operates at $k_f/k_{min} \in [1, 2]$ in all cases shown. If one assumes that a small negative slope $\chi(k) \sim k^{-0.1}$ seen at $k/k_{min} \in [10, 60]$ (which can be traced to some extent in all simulations presented in this figure, see also Fig. 1**e**) is real, i.e. forms as a result of self-organization in supersonic turbulence, then it would seem that an isotropic forcing with $\chi_f \in [0.6, 0.7]$ would be an optimal choice for $M_s \approx 6$. At the same time, the green line in Fig. 1**b** shows that the effects of enforcing $\chi_f = 0$ at

---

[3] http://lca.ucsd.edu/projects/enzo

$k_f/k_{min} \in [1,2]$ are felt at least up to $k = 16k_{min}$, which is substantially larger than k_f. A similar decline towards smaller wavenumbers is seen in the blue and pink curves, corresponding to $M_A = 10$ and 3, respectively. The trans-Alfvénic run at $M_A = 1$ shown in black does not have that feature.

To better recognize the slope in $\chi(k) \sim k^{-0.1}$, we replot the two 1024^3 results in a log-log plot, where it can be seen better (Fig. 1**e**). Is this slope real? Does it depend on the forcing? Is it related to specifics of numerical dissipation at small scales? To address these questions, we explored results of an MHD simulation of decaying turbulence, where the effects of continuous driving are minimized. This 1024^3 PPML simulation was carried out as part of KITP07 code comparison project.[4] The simulation follows a free decay of turbulence from a developed statistical steady state with $M_s \approx 10$ and $M_A \approx 10$ down to $M_s \approx 2$. Figure 1**f** shows $\chi(k)$ for 10 flow snapshots equally spaced in time. As can be seen, with no forcing, the slope of -0.13 ± 0.03 is clearly present even though in this case we only have instantaneous power spectra and the data are rather noisy. In Fig. 1**g** we show $\chi(k)$ obtained for the 5th snapshot at 512^3 and 1024^3 to illustrate grid convergence with PPML. We also compared PPML results with those from three other popular numerical methods and implementations for compressible ideal MHD (ZEUS, FLASH, RAMSES, see Kritsuk et al. 2009c) at a grid resolution of 512^3 zones and found an excellent agreement. It seems that the slope is indeed real and does not depend on forcing or numerical dissipation. We derived a simple fitting formula for $\chi(k)$ in this decaying turbulence model, assuming a fixed slope of -0.13 and fitting a normalization constant $\chi(k/k_{min} = 1)$ against M_s^2, as shown in Fig. 1**h**. The approximation valid in the inertial range for rms turbulent Mach numbers $M_s \in [1, 10]$,

$$\chi(k) \approx \left(0.44 + 0.004M_s^2\right)(k/k_{min})^{-0.13}, \tag{1}$$

is not unique, but still can be used as a guide in future experiments with optimized forcing for supersonic super-Alfvénic turbulence.

3.   Conclusion

We explored the problem of forcing optimization to maximize the effective Reynolds numbers achieved in simulations of supersonic molecular cloud turbulence. Our results demonstrate that for low sonic Mach numbers and/or Alfvénic Mach numbers $M_A \lesssim 1$ solenoidal forcing is reasonable. At the same time, for sonic and Alfvénic Mach numbers above 3, solenoidal forcing is inappropriate, a proper mixture of dilatational and solenoidal modes is required for optimal representation of the inertial range. A purely compressional driving is impractical as it does not allow to study the scaling properties of fully developed supersonic turbulence.

---

[4]`http://kitpstarformation07.wikispaces.com/Star+Formation+Test+Problems`

References

Boldyrev, S., Nordlund, Å., & Padoan, P. 2002a, Phys. Rev. Lett., 89, 031102
Boldyrev, S., Nordlund, Å., & Padoan, P. 2002b, ApJ, 573, 678
Colella P. and Woodward P. R. 1984, J. Comp. Phys., 54, 174
Elmegreen, B. G., & Scalo, J. 2004, ARA&A, 42, 211
Federrath, C., Duval, J., Klessen, R., Schmidt, W., & Mac Low, M.-M. 2009, arXiv:0905.1060
Federrath, C., Klessen, R. S., & Schmidt, W. 2008, ApJL, 688, L79
Heyer, M. H., & Brunt, C. M. 2004, ApJ, 615, L45
Kaplan, S. A. & Pronik, V. I. 1953, Dokl. Akad. Nauk SSSR, 89, 643
Kritsuk, A. G., Ustyugov, S. D., Norman, M. L., Padoan, P. 2009a, ASP Conf. Ser., 406, 15
Kritsuk, A. G., Ustyugov, S. D., Norman, M. L., Padoan, P. 2009b, Journal of Physics: Conf. Ser., 180, 012020
Kritsuk, A. G., Nordlund, Å., Padoan, P., et al. 2009c, KITP07 MHD Code Comparison, in preparation
Kritsuk, A. G., Norman, M. L., Padoan, P. 2007a, ApJ, 665, 416
Larson, R. B. 1981, MNRAS, 194, 809
Mac Low, M.-M., & Klessen, R. S. 2004, Rev. Mod. Phys., 76, 125
McKee, C. F., & Ostriker, E. C. 2007, ARA&A, 45, 565
Nordlund, Å., & Padoan, P. 2003, Lecture Notes in Physics, 614, 271
Pavlovski, G., Smith, M. D., & Mac Low, M.-M. 2006, MNRAS, 368, 943
Padoan, P., & Nordlund, A. 2009, arXiv:0907.0248
Padoan, P., Nordlund, Å., Kritsuk, A., Norman, M., & Li, P. S. 2007, ApJ, 661, 972
Porter, D., Pouquet, A., & Woodward, P. 2002, Phys. Rev. E, 66, 026301
Porter, D., Pouquet, A., Sytine, I., & Woodward, P. 1999, Physica A, 263, 263
Porter, D. H., Pouquet, A., & Woodward, P. R. 1994, Physics of Fluids, 6, 2133
Pouquet, A., Passot, T., & Leorat, J. 1991, in Proc. IAU Symp. 147, "Fragmentation of Molecular Clouds and Star Formation", p. 101
Schmidt, W., Federrath, C., Hupp, M., Kern, S., & Niemeyer, J. C. 2009, A&A, 494, 127
Schmidt, W. 2009, arXiv:0910.0183 (this volume)
Schmidt, W., Federrath, C., & Klessen, R. 2008, Phys. Rev. Lett., 101, 194505
Sytine, I. V., Porter, D. H., Woodward, P. R., Hodson, S. W., & Winkler, K.-H. 2000, J. Comp. Phys., 158, 225
Ustyugov, S. D., Popov, M. V., Kritsuk, A. G., & Norman, M. L. 2009, J. Comp. Phys., 228, 7614